Fermi Surface and Magnetic Properties in Ferromagnet CoS_2 and Paramagnet $CoSe_2$ with the Pyrite-type Cubic Structure

A Teruya[1], F Suzuki[1], D Aoki[2], F Honda[2], A Nakamura[2], M Nakashima[3], Y Amako[3], H Harima[4], K Uchima[5], M Hedo[6], T Nakama[6], and Y Ōnuki[6]

[1]Graduate School of Engineering and Science, University of the Ryukyus, Nishihara, Okinawa 903-0213, Japan
[2]Institute for Materials Research, Tohoku University, Oarai, Ibaraki 311-1313, Japan
[3]Faculty of Science, Shinshu University, Matsumoto, Nagano 390-8621, Japan
[4]Graduate School of Science, Kobe University, Kobe 657-8501, Japan
[5]General Education, Okinawa Christian Junior College, Nishihara, Okinawa 903-0207, Japan
[6]Faculty of Science, University of the Ryukyus, Nishihara, Okinawa 903-0213, Japan

E-mail: uchima@ocjc.ac.jp

Abstract. We succeeded in growing high-quality single crystals of pyrite-type cubic compounds $CoSe_2$ and CoS_2 using a transport agent of $CoBr_2$ and measured the electrical resistivity, specific heat, magnetic susceptibility, magnetization, and the de Haas–van Alphen (dHvA) effect. We confirmed that $CoSe_2$ is an exchange-enhanced paramagnet revealing a broad maximum at around 50 K in the temperature dependence of the magnetic susceptibility. The electronic specific heat coefficient is moderately large, $\gamma = 18$ mJ/(K^2·mol). On the other hand, CoS_2 is a ferromagnet with a Curie temperature $T_C = 122$ K and an ordered moment $\mu_s = 0.93$ μ_B/Co. The γ value of 21 mJ/(K^2·mol) in CoS_2 is slightly larger than that of $CoSe_2$. A large ordered moment, together with a large γ value, is a characteristic feature in CoS_2 because CoS_2 is a half-metallic spin state in the ferromagnetic state. Correspondingly, we detected a main dHvA branch with a large cyclotron effective mass of $13m_0$ in the dHvA experiments. The detected dHvA branches in CoS_2 and $CoSe_2$ are discussed on the basis of the results of energy band calculations, revealing a broken four-fold-symmetry in the angular dependence of the dHvA frequency.

1. Introduction

CoS_2 and $CoSe_2$ belong to the pyrite-type compounds, which were once studied extensively and are still interestingly studied from a viewpoint of a magnetic transition under pressure [1] and the application of spintronics [2]. CoS_2 is a ferromagnet with a Curie temperature $T_C = 124$ K. In CoS_2, the antibonding Co-e_g band is occupied by one $3d$ electron, revealing a quarter filling. An ordered moment of $\mu_s = 0.85$ μ_B/Co with an easy-axis along the [111] direction in CoS_2 is close to 1 μ_B/Co in a low-spin state of Co^{2+} ($S = 1/2$ and $g = 2$). In fact, the magnetic susceptibility follows the Curie–Weiss law above 400 K, with an effective magnetic moment of $\mu_{eff} = 1.76$ μ_B/Co, which corresponds to 1.73 μ_B of Co^{2+} [3, 4]. The de Haas–van Alphen (dHvA) experiment was carried out, detecting the mainly five kinds of dHvA branches

Content from this work may be used under the terms of the Creative Commons Attribution 3.0 licence. Any further distribution of this work must maintain attribution to the author(s) and the title of the work, journal citation and DOI.
Published under licence by IOP Publishing Ltd

with the largest cyclotron mass of about $5m_0$ [5]. On the other hand, $CoSe_2$ is an exchange-enhanced paramagnet. The magnetic susceptibility follows the Curie–Weiss law above 300 K, with $\mu_{\rm eff} = 1.72\ \mu_{\rm B}$/Co [3], which also corresponds to 1.73 $\mu_{\rm B}$/Co of Co^{2+}. These characteristic features including the temperature-induced local moments at high temperatures and itinerant $3d$-electrons at low temperatures are explained by the spin fluctuation theory [6].

In the present dHvA experiments, we detected a large cyclotron effective mass $m_{\rm c}^* = 13m_0$ for a main Fermi surface of CoS_2. This is unexpectedly large because CoS_2 possesses a large ordered moment. The cyclotron mass of CoS_2 is compared with that of $CoSe_2$. The Fermi surfaces obtained from the angular dependences of dHvA frequencies in CoS_2 and $CoSe_2$ are also compared with the results of energy band calculations.

2. Experimental Procedure

Single crystals of CoS_2 were previously grown by the vapor transport method using the chlorine (Cl_2) gas [4, 5]. Recently, $CoBr_2$ was employed as a transport agent [7], revealing the residual resistivity $\rho_0 = 0.86\ \mu\Omega$·cm and the residual resistivity ratio RRR[$= \rho_{\rm RT}/\rho(5\ {\rm K})$] = 160. The CoS_2 powder was set in a hot zone at 700 °C and single crystals were grown in a cold zone at 640 °C. Following this method, we grew single crystals of CoS_2 with 3–4 mm on an edge. The best sample was obtained with $\rho_0 = 0.42\ \mu\Omega$·cm and RRR = 410. Note that RRR was estimated to be 60 in the vapor transport method using Cl_2 in the previous report [4, 5]. Under the same experimental condition, we also grew single crystals of $CoSe_2$. As far as we know, the previous measurements of $CoSe_2$ were carried out using polycrystalline samples. The present results shown below were the first ones using single crystal samples. The direction of the sample was determined by the X-ray Laue method.

The electrical resistivity was measured by the conventional four-terminal DC method. The magnetic susceptibility and the magnetization were measured using a commercial superconducting quantum interference device (SQUID) magnetometer. The specific heat was measured by the quasi-adiabatic heat-pulse method. The dHvA experiment was carried out by the standard field-modulation method with a modulation frequency of 60 Hz and a modulation field of 80 Oe in strong magnetic fields up to 150 kOe.

3. Experimental Results

First, we confirmed the fundamental properties of a paramagnet $CoSe_2$ and a ferromagnet CoS_2 measuring the electrical resistivity, specific heat, magnetic susceptibility, and magnetization. Figure 1(a) shows the temperature dependence of the electrical resistivity for the current along the [100] direction. The resistivity in $CoSe_2$ decreases almost linearly with decreasing temperature. The ρ_0 and RRR are $\rho_0 = 2.1\ \mu\Omega$·cm and RRR = 49, revealing a relatively good single crystal sample.

Next, we measured the specific heat C below 15 K. Figure 1(b) shows the T^2-dependence of the specific heat in the form of C/T. The specific heat in $CoSe_2$ consists of the electronic specific heat γT and phonon contribution $C_{\rm ph} = \beta T^3$ because the magnetic susceptibility becomes approximately constant below 15 K, shown below. The electronic specific heat coefficient γ and the Debye temperature $\Theta_{\rm D}$ are obtained as $\gamma = 18$ mJ/(K^2·mol) and $\Theta_{\rm D} = 340$ K. These values are compared with $\gamma = 11$ mJ/(K^2·mol) and $\Theta_{\rm D} = 345$ K for the polycrystalline sample [8].

Next, we show in Fig. 1(c) the temperature dependence of the magnetic susceptibility χ for three principal directions, [100], [110], and [111] in $CoSe_2$. The magnetic susceptibility increases with decreasing temperature, possesses a broad peak at around 50 K and becomes approximately constant below 15 K. Anisotropy of the susceptibility was not observed among the three directions. Note that the Curie–Weiss law with the effective magnetic moment $\mu_{\rm eff} = 1.72\ \mu_{\rm B}$/Co is observed above 300 K [3], as mentioned in Introduction.

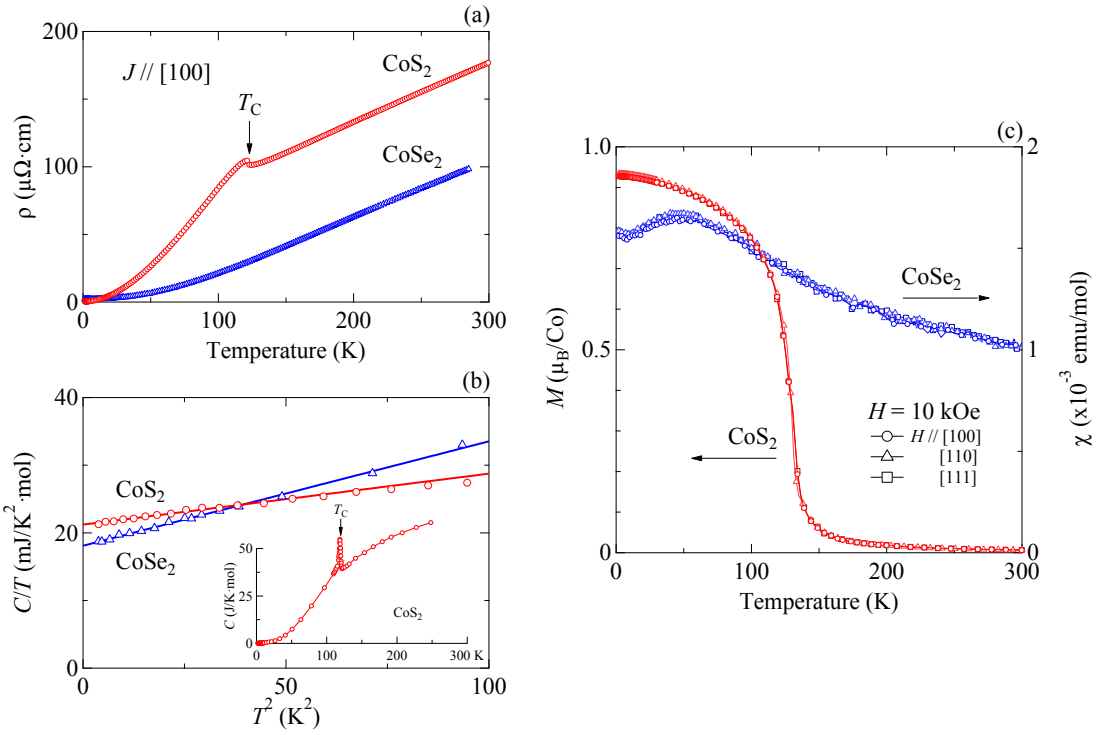


Figure 1. (Color online) Temperature dependences of (a) the electrical resistivity ρ, (b) specific heat C in the form of C/T, and (c) magnetic susceptibility χ and magnetization M in $CoSe_2$ and CoS_2.

Similarly, we measured the electrical resistivity, specific heat, and magnetization M in the ferromagnet CoS_2, as shown in Fig. 1. The ferromagnetic ordering at $T_C = 122$ K is the first-order-like phase transition, revealing sharp peaks in the resistivity and specific heat, as shown in Figs. 1(a) and 1(b). The ρ_0 and RRR are $\rho_0 = 0.42$ $\mu\Omega$·cm and RRR = 410, revealing a high-quality sample. The $\gamma = 21$ mJ/(K^2·mol) is slightly larger than 18 mJ/(K^2·mol) in $CoSe_2$. Note that the previous γ values in CoS_2 are 25.8 mJ/(K^2·mol) [4] and 21.6 mJ/(K^2·mol) [9] for the single crystal samples. The ordered moment μ_s is $\mu_s = 0.93$ μ_B/Co at 2 K, as shown in Fig. 1(c). Note that the saturated moments at 2 K are 0.933 μ_B/Co for $H \parallel [110]$ and 0.928 μ_B/Co for $H \parallel [100]$ and [111], revealing a small difference of 0.005 μ_B/Co between $H \parallel [110]$ and $H \parallel [100]$ and [111]. These values are slightly larger than the previous values of 0.89 μ_B/Co for $H \parallel [100]$ and [111] in the magnetization curve at 4.2 K [4], but are close to 0.91 μ_B/Co in the magnetization curve at 5 K [10] and 0.92(4) μ_B/Co obtained from the polarized neutron scattering experiment at 1.8 K [11]. These cited values were obtained for single crystal samples, which are larger than the value of 0.85 μ_B/Co for the polycrystalline sample mentioned in Introduction [3].

Next, we carried out the dHvA experiment for $CoSe_2$ and CoS_2. Figures 2(a) and 2(b) show the typical dHvA oscillations for $H \parallel [111]$ and the corresponding fast Fourier transformation (FFT) spectrum, respectively, for $CoSe_2$. Four dHvA branches named β, γ, $\varepsilon_{1,2}$, and δ branches are observed. The dHvA frequency F is in the range from 0.548×10^7 to 2.517×10^7 Oe. Here, the dHvA frequency $F(= c\hbar S_F/2\pi e)$ is proportional to the maximum or minimum cross-sectional area of the Fermi surface S_F, which is shown as a unit of magnetic field. We determined the cyclotron masses m_c^* for these branches from the temperature dependences of the dHvA amplitudes. The cyclotron mass, which is described in Fig. 2(b), is in the range from 0.9 to

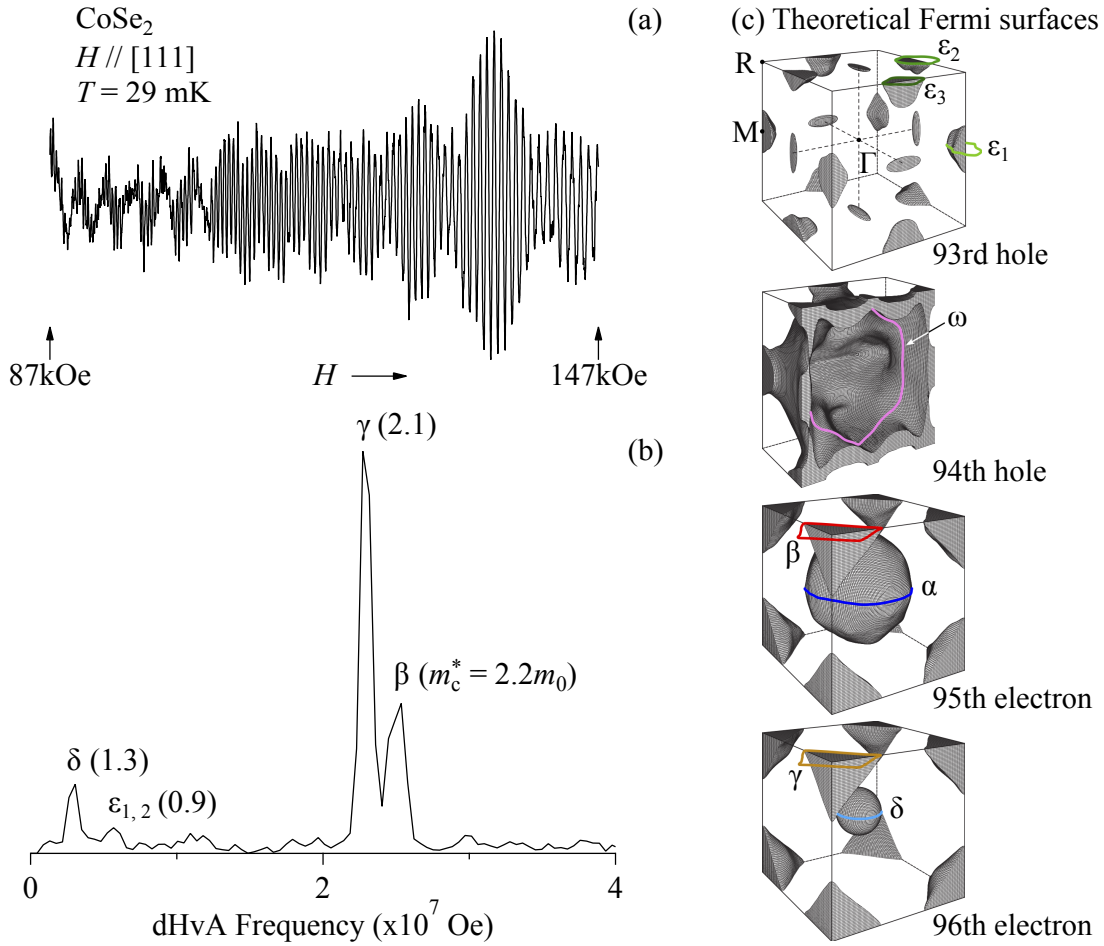


Figure 2. (Color online) (a) Typical dHvA oscillations and (b) the corresponding FFT spectrum for $H \parallel [111]$, and (c) theoretical Fermi surfaces in $CoSe_2$. Figures in parentheses are cyclotron effective masses for dHvA branches.

$2.2m_0$, revealing moderately large masses because the corresponding dHvA frequencies are small in magnitude, namely corresponding to small Fermi surfaces.

To clarify the present experimental results, we carried out the full-potential linearized augmented plane wave (FLAPW) energy band calculations with local density approximation (LDA) for the exchange correlation potential for $CoSe_2$ using the lattice constant $a = 5.8593$ Å and the x parameter of 0.3795 for Se in ref. [12]. In the band calculations, the scalar relativistic effect was taken into account for all the electrons and the spin–orbit interaction was included self-consistently for all the valence electrons as in a second variational procedure. $3p^6 3d^7 4s^2$ electrons for Co and $3d^{10} 4s^2 4p^4$ electrons for Se are treated as valence electrons. Thus, the obtained theoretical Fermi surfaces are shown in Fig. 2(c). The Fermi surfaces consist of band 93rd and 94th hole Fermi surfaces and the compensated band 95th and 96th electron Fermi surfaces. Note that the unit cell contains four molecules of $CoSe_2$ and then electrons are even in number, meaning equal volumes of the hole and electron Fermi surfaces. The detected dHvA branches are identified from the results of band calculations, as follows: (1) branch β is due to a nearly spherical band 95th electron Fermi surface centered at the R point, (2) branch γ is due to a nearly spherical band 96th electron Fermi surface centered at the R point, (3) branches ε_i ($i = 1, 2, 3$) are due to nearly spherical band 93rd hole Fermi surfaces centered at the M point,

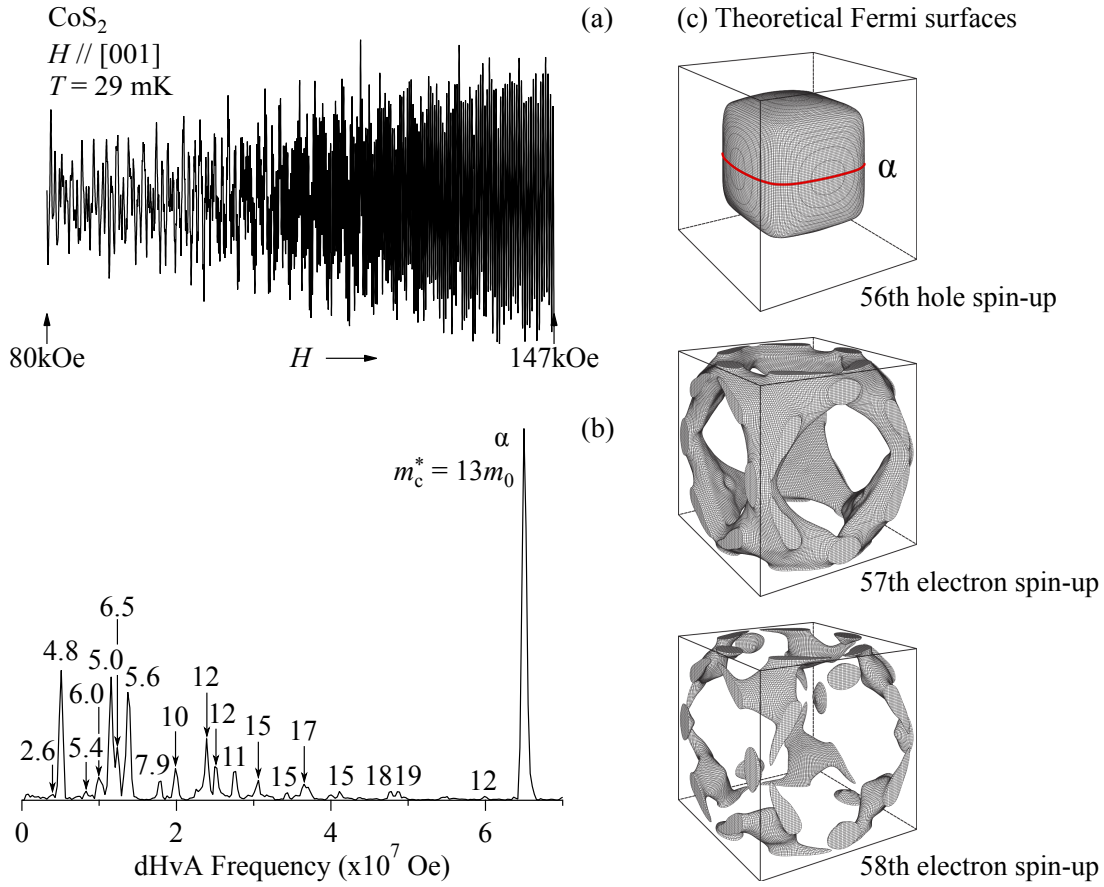


Figure 3. (Color online) (a) Typical dHvA oscillations and (b) the corresponding FFT spectrum, and (c) theoretical Fermi surfaces in CoS_2. Figures in (b) correspond to the cyclotron effective masses, for example $13m_0$ for branch α.

(4) branch δ is due to a spherical band 96th electron Fermi surface centered at the Γ point, although the theoretical Fermi surface is larger than the experimental one in volume, and (5) theoretically, much larger Fermi surfaces exist, which are due to a nearly spherical band 95th electron Fermi surface named α and a multiply-connected band 94th hole Fermi surfaces with vacant space in center. These branches were not observed experimentally mainly because of large cyclotron masses of (10–20m_0) and a quality of the sample (RRR = 49).

We show later in Fig. 4(a) the total and partial densities of states in $CoSe_2$. As discussed in Introduction, the bonding e_g band spreads widely in the energy range from 0 to 0.35 Ry, the t_{2g} band forms a very narrow band around 0.40–0.45 Ry, and the antibonding e_g band spreads from 0.5 to 0.7 Ry in energy. All these bands are formed mainly from contributions of Co-3d and Se-4p electrons. A dominant contribution is due to Co-3d electrons. A quarter-filled e_g band is characteristic in the density of states, revealing a large density of states at Fermi energy in a narrow band. The theoretical γ_b value is $\gamma_b = 6.93$ mJ/(K^2·mol). The experimental γ value of 18 mJ/(K^2·mol) is by 2.6 times larger than the theoretical one.

Similarly, we carried out the dHvA experiments for the ferromagnet CoS_2. Figures 3(a) and 3(b) show the typical dHvA oscillations in the ferromagnetic state of CoS_2 and the corresponding FFT spectrum, respectively. A main dHvA branch named α possesses a dHvA frequency of 6.506×10^7 Oe. The cyclotron effective mass is unexpectedly large, $13m_0$. The other branches are also large, ranging from 2.6 to $19m_0$.

Figure 3(c) shows the theoretical Fermi surfaces. Here, the present band calculations were carried out using the FLAPW method within the local spin density approximation where the ferromagnetic state is assumed, but the spin-orbit interaction is neglected for simplicity. The lattice parameters are adopted from ref. [13], namely $a = 5.5385$ Å and $x = 0.38988$ for S. $3p^6 3d^7 4s^2$ electrons for Co and $3s^2 3p^4$ electrons for S are treated as valence electrons.

It is characteristic that Fermi surfaces are constructed only from the spin-up band. The Fermi energy is located just below the antibonding e_g band with the spin-down state, revealing a half-metallic spin state. The Fermi surfaces in Fig. 3(c) is thus based on the 56th hole spin-up band and the compensated 57th electron spin-up and 58th electron spin-up bands. Note that the theoretical dHvA frequency of branch α for $H \parallel [001]$ is $F_{\rm b} = 6.352 \times 10^7$ Oe, which is close to the experimental value of $F = 6.506 \times 10^7$ Oe, while the corresponding band mass of $m_{\rm b} = 0.68 m_0$ is compared with the experimental value of $m_{\rm c}^* = 13 m_0$. Theoretically, Co-3d electrons produce a magnetic moment of 0.88 $\mu_{\rm B}$/Co.

4. Concluding Remark

Finally, we discuss the ferromagnetic ordering and the Fermi surface properties in CoS_2. Figures 4(a), 4(b), 4(c), and 4(d) show the total and partial densities of states in $CoSe_2$, the Co-3d partial density of states in the paramagnetic state of CoS_2, and the Co-3d partial densities of states in the ferromagnetic spin-up and -down states of CoS_2, respectively. Note that the Co-3d partial density of states is roughly the same between CoS_2 and $CoSe_2$ in the paramagnetic state. Correspondingly, the theoretical $\gamma_{\rm b}$ value of 6.62 mJ/(K^2·mol) in the paramagnetic state of CoS_2 is approximately the same as $\gamma_{\rm b} = 6.93$ mJ/(K^2·mol) in $CoSe_2$. Important is that the band width below the Fermi energy in the paramagnetic state of CoS_2 is much narrower than that in $CoSe_2$. Moreover, there exists a much larger Co-3d partial density of states below the Fermi energy in the paramagnetic state of CoS_2, which produces a ferromagnetic ordering at low temperatures in CoS_2. Note that the theoretical $\gamma_{\rm b}$ value in the ferromagnetic state is 3.03 mJ/(K^2·mol), which is smaller than $\gamma_{\rm b} = 6.62$ mJ/(K^2·mol) in the paramagnetic state. The present small theoretical value of $\gamma_{\rm b} = 3.03$ mJ/(K^2·mol) in the ferromagnetic state is compared with the experimental value of $\gamma = 21$ mJ/(K^2·mol), revealing a large enhancement of the γ value, $\gamma/\gamma_{\rm b} = 7$. From these experimental results, an electronic state of CoS_2 is close to a quantum critical point, which is defined as an electronic state of $T_{\rm C} \to 0$. In fact, the Curie temperature becomes zero in $Co(S_{1-x}Se_x)_2$ with $x = 0.11$ [14].

Moreover, as shown in Fig. 4(c), only the spin-up state in the e_g band is occupied by the Co-3d electrons, while the spin-down state is empty, revealing the half-metallic spin state. This is a main reason why the large ordered moment of $\mu_{\rm s} = 0.93$ $\mu_{\rm B}$/Co is realized in CoS_2. It is thus concluded that a large ordered moment, together with a large γ value, is a characteristic feature in CoS_2.

Acknowledgments

We are very grateful to Prof. K. Ueda for helpful discussions. This work was supported by JSPS KAKENHI Grant Numbers 15H05884, 25247055, and 15H05886.

References

[1] Sidorov V A, Krasnorussky V N, Petrova A E, Utyuzh A N, Yuhasz W M, Lograsso T A, Thompson J D and Stishov S M 2011 *Phys. Rev.* B **83** 060412
[2] Leighton C, Manno M, Cady A, Freeland J W, Wang L, Umemoto K, Wentzcovitch R M, Chen T Y, Chien C L, Kuhns P L, Hoch M J R, Reyes A P, Moulton W G, Dahlberg E D, Checkelsky J and Eckert J 2007 *J. Phys.: Condens. Matter* **19** 315219
[3] Adachi K, Sato K and Takeda M 1969 *J. Phys. Soc. Jpn.* **26** 631
[4] Hiraka H and Endoh Y 1994 *J. Phys. Soc. Jpn.* **63** 4573

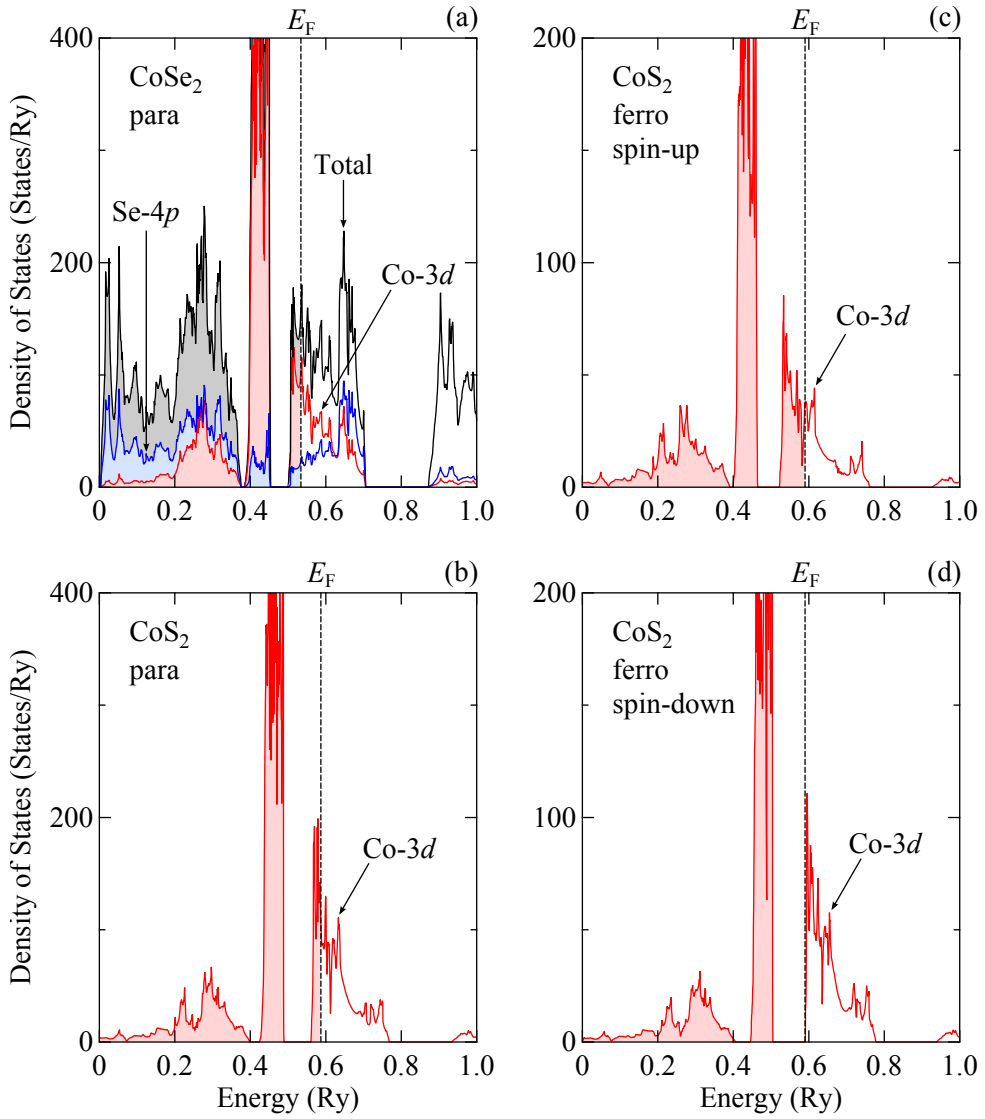


Figure 4. (Color online) Total and partial densities of states in (a) the paramagnetic $CoSe_2$, (b) Co-3d partial densities of states in the paramagnetic CoS_2, and (c) and (d) the ferromagnetic CoS_2.

[5] Ishiguro A, Sawada A, Suzuki M, Hiraka H, Yamada K, Endoh Y and Komatsubara T 1998 *J. Magn. Magn. Mater.* **177–181** 1355
[6] Moriya T 1985 *Spin Fluctuations in Itinerant Electron Magnetism* (Berlin Heidelberg: Springer-Verlag) p 152
[7] Wang L, Chen T Y, Chien C L and Leighton C 2006 *Appl. Phys. Lett.* **88** 232509
[8] Ogawa S and Nishihara Y 1977 *J. Phys. Soc. Jpn.* **42** 343
[9] Otero-Leal M, Rivadulla F, García-Hernández M, Piñeiro A, Pardo V, Baldomir D and Rivas J 2008 *Phys. Rev.* B **78** 180415
[10] Yamamoto R, Machida A, Moritomo Y and Nakamura A 1999 *Phys. Rev.* B **59** R7793
[11] Brown P J, Neumann K-U, Simon A, Ueno F and Ziebeck K R A 2005 *J. Phys.: Condens. Matter* **17** 1583
[12] Furuseth S, Kjekshus A and Andresen A F 1969 *Acta Chem. Scand.* **23** 2325
[13] Nowack E, Schwarzenbach D and Hahn T 1991 *Acta Crystallogr.* B **47** 650
[14] Goto T, Shindo Y, Takahashi H and Ogawa S 1997 *Phys. Rev.* B **56** 14019